Supplementary Information for

# Light-Induced Spin-State Switching in Fe(II) Spin-Crossover Complexes with Thiazole-Based Chelating Ligands

Minyoung Jo,[a] Botagoz Amanyazova,[a,b] Sandugash Yergeshbayeva,[a] Miguel Gakiya-Teruya,[a] Ökten Üngör,[a,#] Paola Lopez Rivera,[a,c] Natalie Jen,[a] Evgeny Lukyanenko,[d] Alexander V. Kurkin,[d] Rakhmetulla Erkasov,[b] Mark W. Meisel,[e] Andreas Hauser,[f] Pradip Chakraborty,[g] Michael Shatruk[a,*]

[a] *Department of Chemistry and Biochemistry, Florida State University, Tallahassee, Florida 32306, United States*
[b] *Department of Chemistry, L.N. Gumilyov Eurasian National University, Astana 010008, Kazakhstan*
[c] *Department of Chemistry, University of Puerto Rico at Humacao, Humacao, PR 00792, Puerto Rico*
[d] *Department of Chemistry, Lomonosov Moscow State University, Moscow, 119234, Russia*
[e] *Department of Physics and National High Magnetic Field Laboratory, University of Florida, Gainesville, Florida 32611, United States*
[f] *Department of Physical Chemistry, University of Geneva, CH-1211 Geneva 4, Switzerland*
[g] *Department of Chemistry, Indian Institute of Technology, Kharagpur 721 302, India*

* Corresponding authors: shatruk@chem.fsu.edu, pradipc@chem.iitkgp.ac.in

**Contents:**

**Table S1.** Data collection and structure refinement parameters for **1**, **2**·MeOH, and **3**·2(3tpH).

| Compound | $FeCl_2S_6O_8N_6C_{18}H_{12}$ | $FeCl_2S_6O_9N_6C_{19}H_{16}$ | | | $FeCl_2S_5O_8N_{15}C_{30}H_{25}$ | | |
|---|---|---|---|---|---|---|---|
| | [**1**] | [**2**·MeOH] | | | [**3**·2(3tpH)] | | |
| Temperature, K | 300 K | 300 K | 230 K | 100 K | 300 K | 230 K | 100 K[b] |
| CCDC number | 2325289 | 2325294 | 2325293 | 2325292 | 2325291 | 2325290 | 2325295 |
| Formula weight | 759.45 | 791.49 | 791.49 | 791.49 | 1010.70 | 1010.70 | 1010.70 |
| Space group | *C*2/*c* | $P2_1/n$ | $P2_1/n$ | $P2_1/n$ | *Pbcn* | *Pbcn* | $Pna2_1$ |
| *a*, Å | 17.2500(3) | 9.7717(2) | 9.7514(2) | 9.9078(1) | 15.0200(9) | 14.9806(6) | 17.8075(6) |
| *b*, Å | 9.8245(2) | 22.8622(4) | 22.6547(3) | 21.8512(3) | 15.627(1) | 15.5610(6) | 15.1011(3) |
| *c*, Å | 16.8597(3) | 13.2779(3) | 13.1878(2) | 12.7772(2) | 17.792(1) | 17.7708(7) | 44.5307(8) |
| $\alpha$, deg | 90 | 90 | 90 | 90 | 90 | 90 | 90 |
| $\beta$, deg | 105.972(2) | 90.532(2) | 90.540(1) | 90.013(1) | 90 | 90 | 90 |
| $\gamma$, deg | 90 | 90 | 90 | 90 | 90 | 90 | 90 |
| *V*, $Å^3$ | 2746.96(9) | 2966.2(1) | 2913.25(8) | 2766.23(6) | 4176.0(5) | 4142.6(3) | 11974.9(5) |
| *Z* | 4 | 4 | 4 | 4 | 4 | 4 | 12 |
| Crystal color | red | light-red | light-red | red | yellow | yellow | red |
| Crystal size, $mm^3$ | 0.24×0.15×0.13 | 0.44×0.28×0.21 | 0.44×0.28×0.21 | 0.33×0.19×0.16 | 0.49×0.33×0.18 | 0.25×0.15×0.14 | 0.37×0.14×0.12 |
| $d_{calc}$, g $cm^{-3}$ | 1.836 | 1.772 | 1.805 | 1.823 | 1.606 | 1.621 | 1.682 |
| $\mu$, $mm^{-1}$ | 10.979 | 1.170 | 1.191 | 1.255 | 0.807 | 0.813 | 0.844 |
| $\lambda$, Å | 1.54184 | 0.71073 | 0.71073 | 0.71073 | 0.71073 | 0.71073 | 0.71073 |
| $2\theta_{max}$, deg | 52.57 | 61.01 | 57.4 | 56.56 | 61.22 | 56.56 | 52.74 |
| Total reflections ($R_{int}$) | 9008 (0.031) | 57061 (0.033) | 53446 (0.029) | 47278 (0.048) | 18931 (0.040) | 25464 (0.027) | 170932 (0.083) |
| Unique reflections | 2725 | 9023 | 7508 | 6844 | 5174 | 5129 | 24344 |
| Parameters refined | 186 | 389 | 389 | 390 | 349 | 342 | 872 |
| Restraints used | 0 | 1 | 1 | 1 | 18 | 8 | 13 |
| $R_1$, $wR_2$ [$I > 2\sigma(I)$][a] | 0.039, 0.107 | 0.038, 0.103 | 0.029, 0.076 | 0.049, 0.103 | 0.044, 0.114 | 0.046, 0.111 | 0.149, 0.415 |
| $R_1$, $wR_2$ (all data) | 0.042, 0.109 | 0.051, 0.111 | 0.034, 0.079 | 0.058, 0.107 | 0.096, 0.135 | 0.062, 0.118 | 0.158, 0.422 |
| Goodness of fit[b] | 1.068 | 1.084 | 1.046 | 1.177 | 1.029 | 1.072 | 1.853 |
| Diff. peak/hole, e $Å^{-3}$ | 0.32, –0.42 | 0.42, –0.42 | 0.75, –0.46 | 0.58, –0.49 | 0.25, –0.27 | 0.43, –0.31 | 3.66, –1.48 |

[a] $R_1 = \Sigma||F_o|-|F_c||/\Sigma|F_o|$; $wR_2 = [\Sigma[w(F_o^2-F_c^2)^2]/\Sigma[w(F_o^2)^2]]^{½}$; [b] Goodness-of-fit = $[\Sigma[w(F_o^2-F_c^2)^2]/(N_{obs}-N_{params})]^{½}$, based on all data.

[b] The determination of the crystal structure of **3**·2(3tpH) at 100 K was thwarted by poor quality of the diffraction data caused by cracking of the crystal during the spin transition that led to abrupt structural changes. Nevertheless, the structural model provides a reliable estimate for the Fe–N bond lengths given in Table 1.

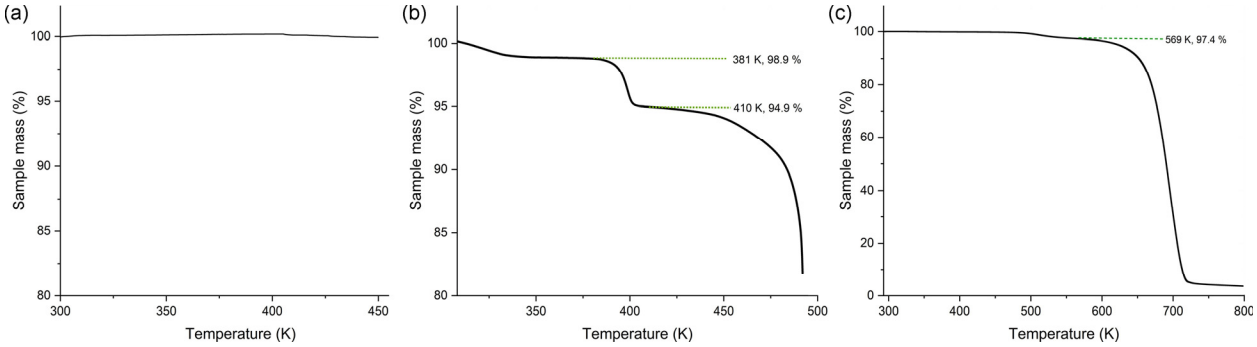


**Figure S1.** Thermogravimetric curves for **1** (a), **2**·MeOH (b), and **3**·2(3tpH) (c).

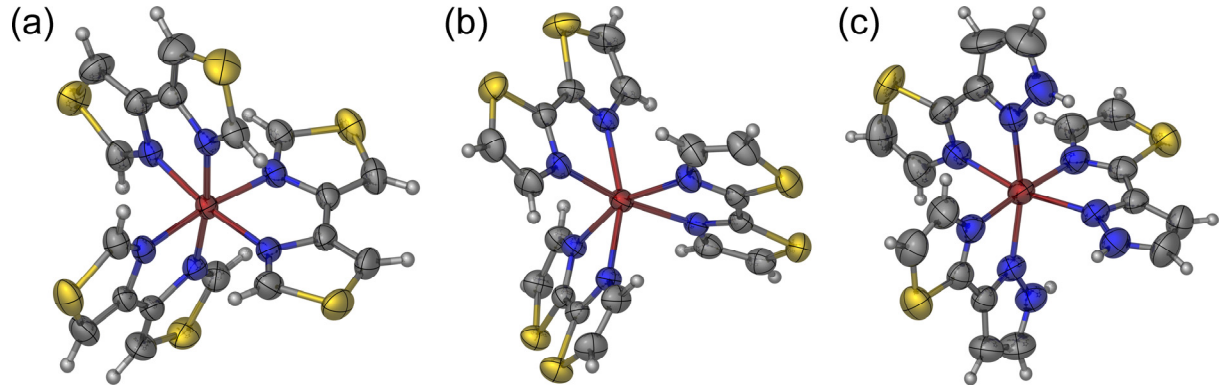


**Figure S2.** The $[Fe(L)_3]^{2+}$ cations in the crystal structures of **1** (a), **2**·MeOH (b), and **3**·2(3tpH) (c). The color scheme: Fe = garnet, S = gold, N = blue, C = gray, H = off-white.

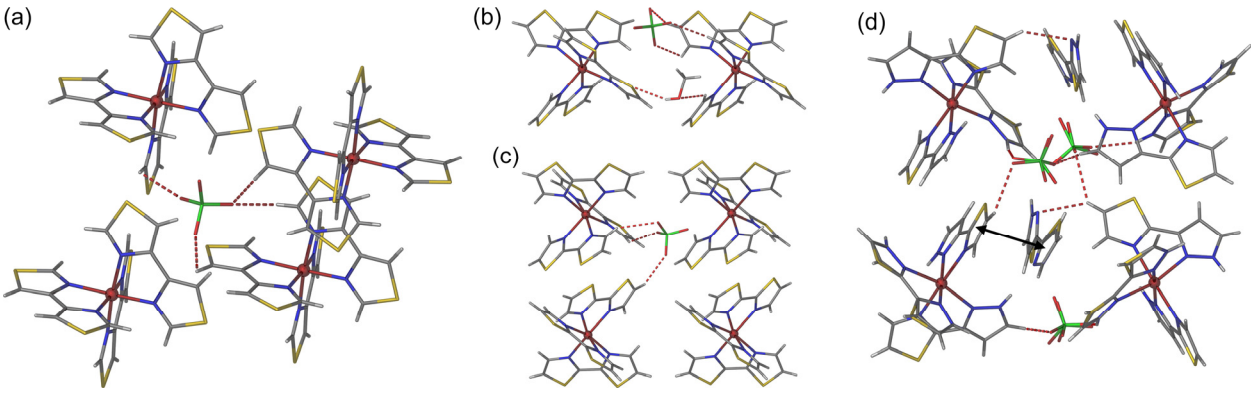


**Figure S3.** Intermolecular interactions (highlighted with dashed lines) in the crystal structures of **1** (a), **2**·MeOH (b, c), and **3**·2(3tpH) (d). Color scheme: Fe = garnet, S = gold, N = blue, C = gray, H = off-white.

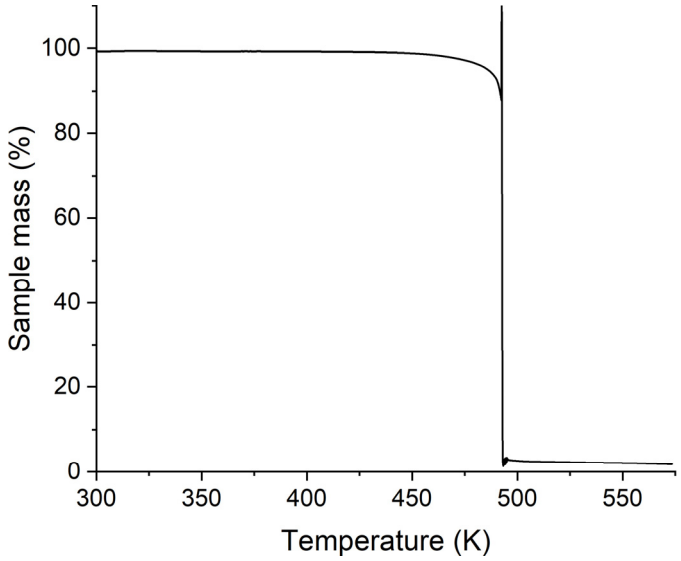


**Figure S4.** Thermogravimetric curve for **2**·MeOH after magnetic measurements, indicating the absence of any mass loss due to interstitial solvent. The spike and abrupt mass loss at 490 K are caused by explosive decomposition of the perchlorate-containing complex.

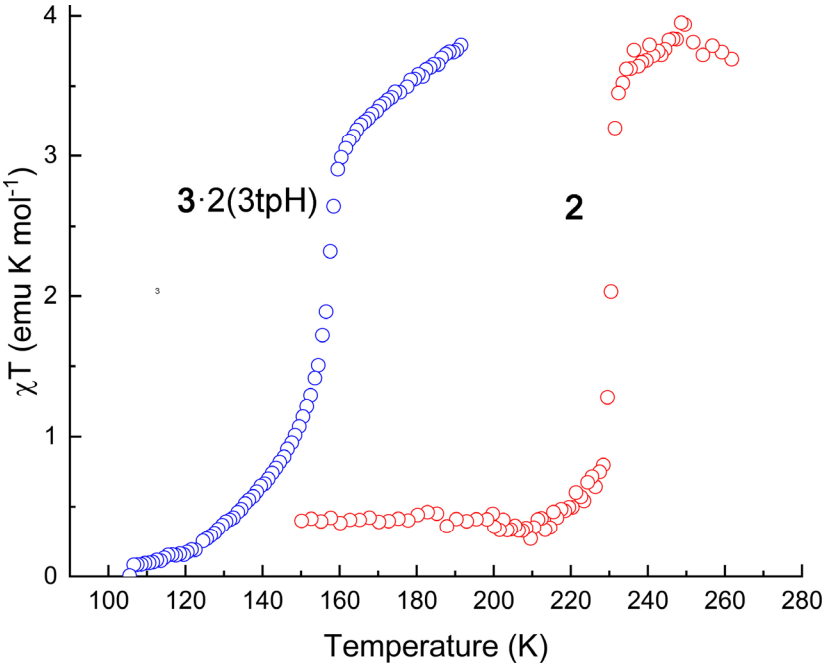


**Figure S5.** The temperature dependence of $\chi T$ measured during cooling of samples of **2** and **3**·2(3tpH) prior to photomagnetic measurements. The cooling rate was 2 K/min. For both samples, the thermal SCO occurs at the same temperatures as observed in bulk magnetic measurements (Figure 4 in the main text).

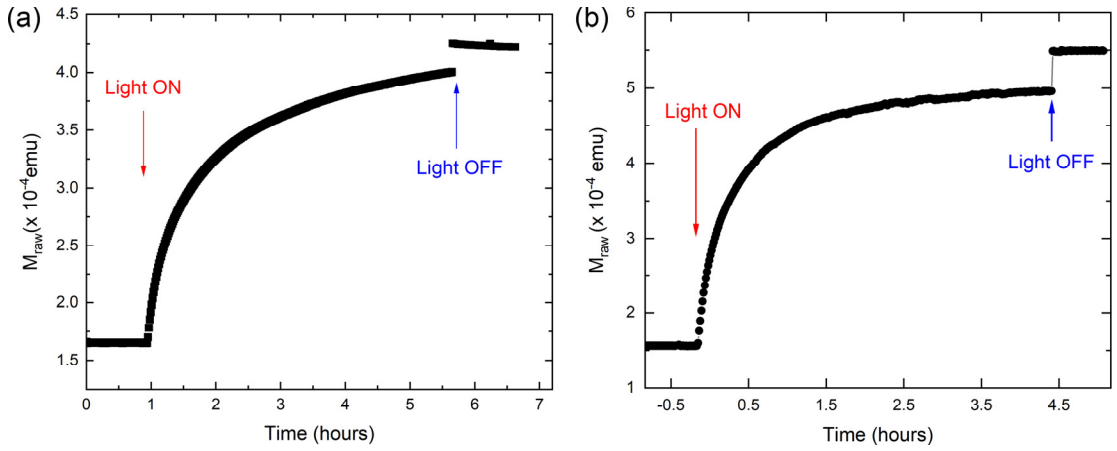


**Figure S6.** Evolution of magnetization upon irradiation of powder samples of **2** (a) and **3**·2(3tpH) (b) with a broadband "white" light at 5 K. The jump in magnetization after the light has been turned off is due to the dissipation of the small amount of heat caused by the irradiation. To allow for thermal equilibration, the measurements in the warming mode (Figure 5) were started 30 min after irradiation had been stopped.

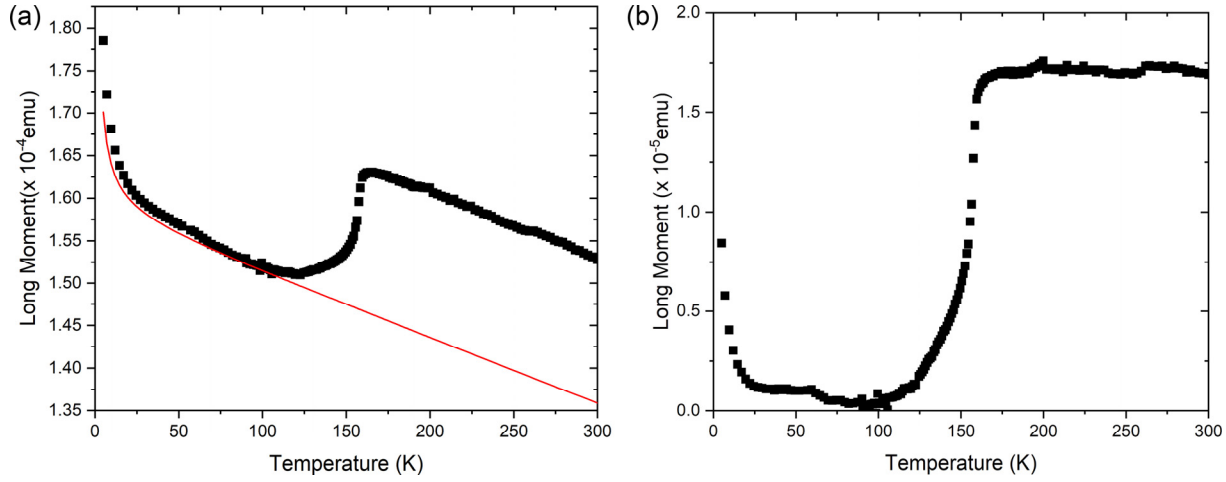


**Figure S7.** An example of the photomagnetic sample holder correction performed on the sample of **3**·2(3tpH). The measured raw magnetization data and the data obtained after correction are shown in panels (a) and (b), respectively. The equation used for the correction is explained below.

The samples used for photomagnetic measurements were thin layers of powder sandwiched between small pieces of Scotch Magic™ tape. Accurate mass determination for such samples was challenging. Therefore, the mass was determined by matching the thermal SCO behavior to that of bulk samples (Figures 4b and 4c in the main text). Doing so required, first of all, correcting the raw magnetic data (Figure S5a) for the contribution from the fiberoptic sample holder (FOSH). The latter was modeled by the equation $M_{\mathrm{FOSH}} = A + \frac{B}{T} - CT$, where the last term represents the temperature-independent paramagnetism both above and below the spin transition, the middle term represents the Curie-type paramagnetism below the transition (where the SCO material in the LS state is expected to show negligible paramagnetism), and the first term is a height-adjustment factor. The data so corrected gave reasonably appearing SCO curves, as shown in Figure S5b. The peak around 50 K was observed in all measurements and increased in magnitude with time. Therefore, this peak was attributed to oxygen impurity that sipped into the sample chamber due

to imperfect hermeticity of the FOSH. The peak was fit by a Gaussian-type curve and subtracted from the measured signal. Finally, the curves were scaled, by adjusting the mass of the sample, to reproduce the thermal SCO observed for the bulk samples. Importantly, the sample masses so determined gave reasonable $\chi T$ values for the light-induced metastable HS states (Figure 5).

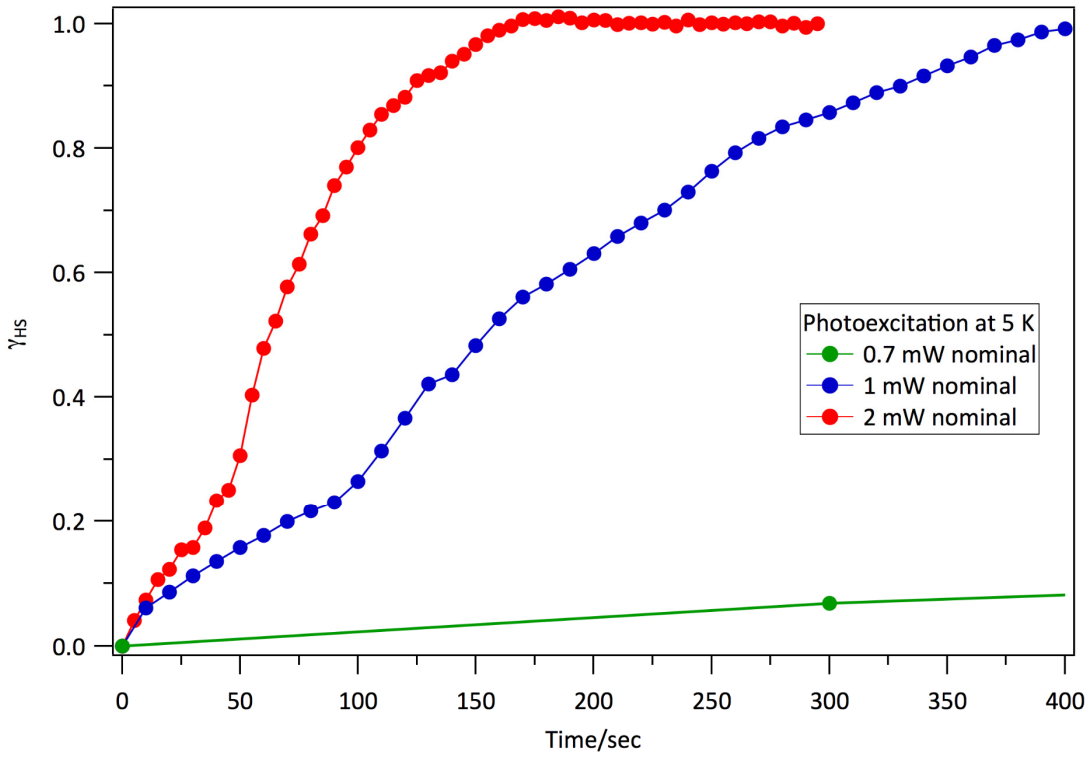


**Figure S8.** The evolution of the HS fraction upon irradiation of a single crystal of **3**·2(3tpH) with a 532 nm laser at 5 K. The power of the laser was varied systematically to determine the optimal excitation conditions.

The photoexcitation curves (Figure S5) were obtained by converting the time-dependent variation of the amplitude of the LS $^1A_1 \rightarrow {}^1T_1$ ligand-field absorption band, monitored at 590 nm, to the fraction of the light-induced HS state, according to Eq. (1) in the main text. At 5 K, the HS $\rightarrow$ LS relaxation is extremely slow; therefore, the photoexcitation to the HS state is not in competition with the relaxation process. At the lower laser power, the photoexcitation is inefficient, achieving less than 10% LS $\rightarrow$ HS conversion after 400 s. Increasing the power above 1 mW results in faster and complete LS $\rightarrow$ HS conversion within 300-400 s. The sigmoidal increase in the fraction of the HS state is due to self-accelerated growth of the HS domains as a result of the moderately strong cooperative effects.

[For examples, see Krivokapic, I.; Enachescu, C.; Bronisz, R.; Hauser, A. *Chem. Phys. Lett.* **2008**, *455*, 192; Chong, C.; Slimani, A.; Varret, F.; Boukheddaden, K.; Collet, E.; Ameline, J. C.; Bronisz, R.; Hauser, A. *Chem. Phys. Lett.* **2011**, *504*, 29.]

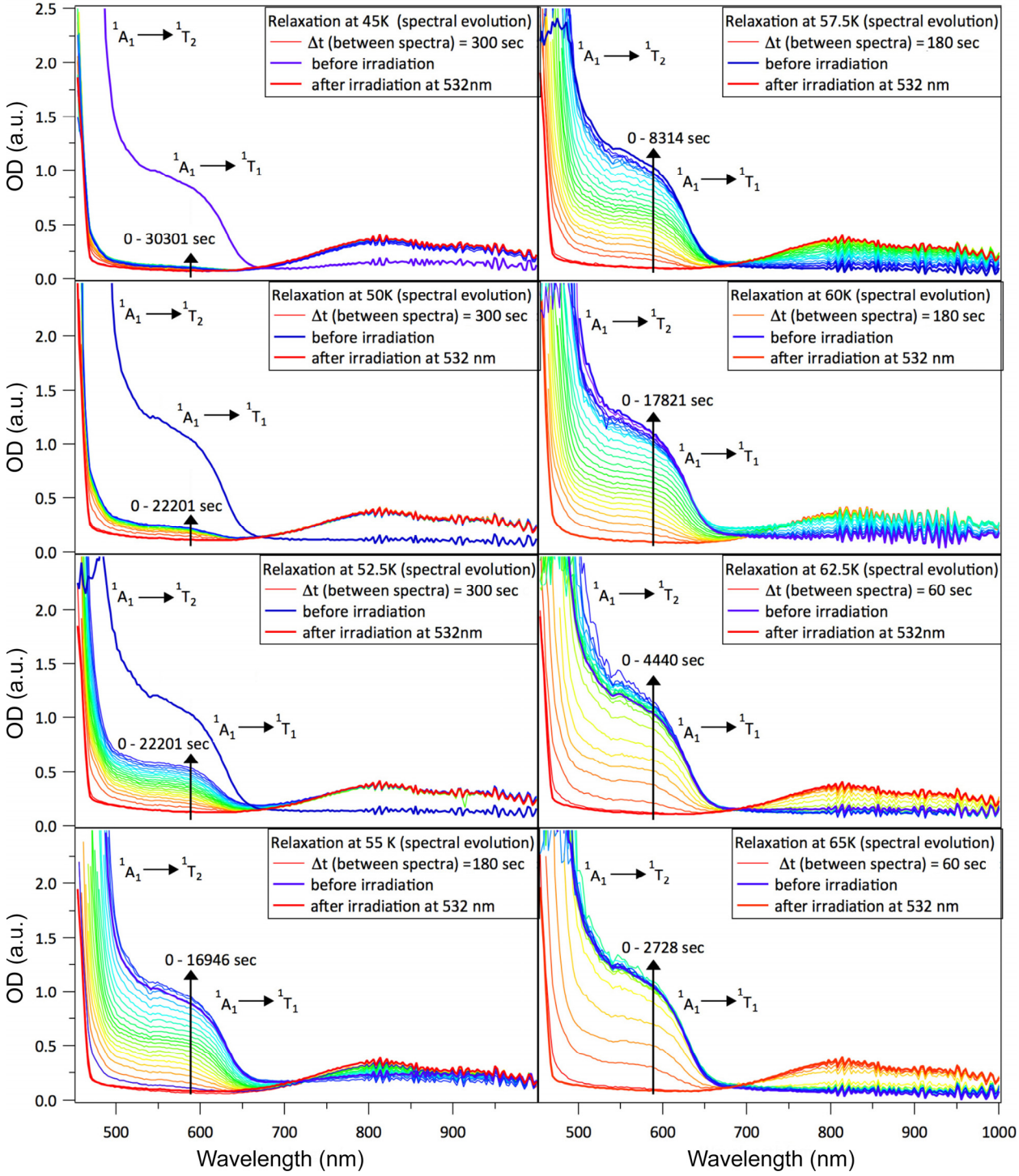


**Figure S9.** Optical absorption spectra showing the relaxation of the LIESST state of **3**·2(3tpH) recorded at different temperatures after the light-induced LS → HS conversion achieved at 5 K. The spectra of the LS state before irradiation and the HS state immediately after irradiation, recorded at 5 K, are shown with the thicker blue and red traces, respectively. The other spectra, evolving as a function of time at a specific indicated temperature, are shown with rainbow-colored thinner traces.